Hyperfine Interact
DOI 10.1007/s10751-011-0456-8

Antihydrogen detection in ALPHA

Richard Hydomako · Gorm Bruun Andresen · Mohammad Dehghani Ashkezari · Marcelo Baquero-Ruiz · William Bertsche · Eoin Butler · Paul David Bowe · Claudo Lenz Cesar · Steve Chapman · Michael Charlton · Joel Fajans · Tim Friesen · Makoto C. Fujiwara · David Russell Gill · Jeffrey Scott Hangst · Walter Newbold Hardy · Ryugo S. Hayano · Michael Edward Hayden · Andrew James Humphries · Svante Jonsell · Leonid Kurchaninov · Niels Madsen · Scott Menary · Paul Nolan · Konstantin Olchanski · Arthur Olin · Alexander Povilus · Petteri Pusa · Francis Robicheaux · Elazar Sarid · Daniel Miranda Silveira · Chukman So · James William Storey · Robert Ian Thompson · Dirk Peter van der Werf · Jonathan Syrkin Wurtele · Yasunori Yamazaki · ALPHA Collaboration

R. Hydomako (✉) · T. Friesen · M. C. Fujiwara · R. I. Thompson
Department of Physics and Astronomy, University of Calgary, Calgary AB, T2N 1N4, Canada
e-mail: rhydomako@phas.ucalgary.ca

G. B. Andresen · P. D. Bowe · J. S. Hangst
Department of Physics and Astronomy, Aarhus University, 8000 Aarhus C, Denmark

M. D. Ashkezari · M. E. Hayden
Department of Physics, Simon Fraser University, Burnaby BC, V5A 1S6, Canada

M. Baquero-Ruiz · S. Chapman · J. Fajans · A. Povilus · C. So · J. S. Wurtele
Department of Physics, University of California, Berkeley, CA 94720-7300, USA

W. Bertsche · M. Charlton · A. J. Humphries · N. Madsen · D. P. van der Werf
Department of Physics, Swansea University, Swansea SA2 8PP, UK

E. Butler
European Laboratory for Particle Physics, CERN, 1211 Geneva 23, Switzerland

C. L. Cesar
Instituto de Fsica, Universidade Federal do Rio de Janeiro, Rio de Janeiro 21941-972, Brazil

M. C. Fujiwara · D. R. Gill · L. Kurchaninov · K. Olchanski · A. Olin · J. W. Storey
TRIUMF, 4004 Wesbrook Mall, Vancouver BC, V6T 2A3, Canada

W. N. Hardy
Department of Physics and Astronomy, University of British Columbia, Vancouver BC, V6T 1Z4, Canada

R. S. Hayano
Department of Physics, University of Tokyo, Tokyo 113-0033, Japan

S. Jonsell
Fysikum, Stockholm University, 10609 Stockholm, Sweden

Published online: 18 November 2011

Abstract The ALPHA project is an international collaboration, based at CERN, with the experimental goal of performing precision spectroscopic measurements on antihydrogen. As part of this endeavor, the ALPHA experiment includes a silicon tracking detector. This detector consists of a three-layer array of silicon modules surrounding the antihydrogen trapping region of the ALPHA apparatus. Using this device, the antihydrogen annihilation position can be determined with a spatial resolution of better than 5 mm. Knowledge of the annihilation distribution was a critical component in the recently successful antihydrogen trapping effort. This paper will describe the methods used to reconstruct annihilation events in the ALPHA detector. Particular attention will be given to the description of the background rejection criteria.

Keywords Antihydrogen · Event reconstruction · Silicon vertex detector · Cosmic background rejection

1 Introduction

The ALPHA experiment, an international collaboration based at CERN's Antiproton Decelerator (AD), is engaged in the production and magnetic confinement of antihydrogen [1]. The creation and capture of antihydrogen opens up an inviting opportunity to test, to a high level of precision, the symmetry between matter and antimatter in the atomic sector. Specifically, the comparison between the atomic spectra of hydrogen (which is very well studied; the $1S - 2S$ transition, for example, is known to parts in 10^{14} [2]) and antihydrogen is a test of the $\mathcal{CPT}$ (Charge-Parity-Time reversal) symmetry [3]. This paper focuses on ALPHA's silicon tracking detector and the methods used to detect and locate magnetically trapped antihydrogen in the ALPHA apparatus.

S. Menary
Department of Physics and Astronomy, York University, Toronto, ON M3J 1P3, Canada

P. Nolan · P. Pusa
Department of Physics, University of Liverpool, Liverpool L69 7ZE, UK

F. Robicheaux
Department of Physics, Auburn University, Auburn, AL 36849-5311, USA

E. Sarid
Department of Physics, NRCN-Nuclear Research Center Negev, Beer Sheva 84190, Israel

D. M. Silveira · Y. Yamazaki
Atomic Physics Laboratory, RIKEN Advanced Science Institute, Wako, Saitama 351-0198, Japan

D. M. Silveira · Y. Yamazaki
Graduate School of Arts and Sciences, University of Tokyo, Tokyo 153-8902, Japan

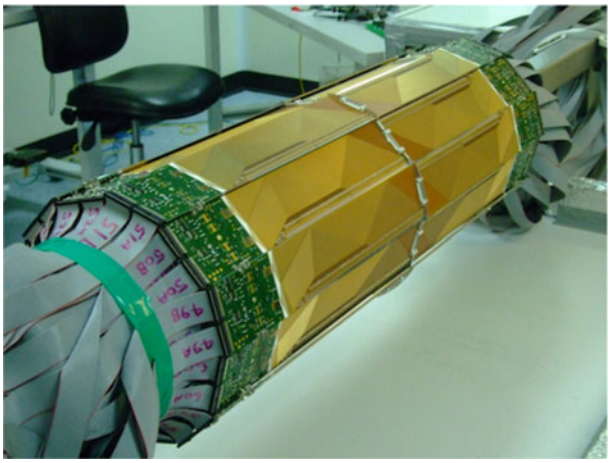

Fig. 1 The ALPHA silicon detector. The *line segments within the gold rectangles* are the leads connecting the microstrips to the readout electronics (the silicon wafers and microstrips are located on the opposite side of the modules and are not seen). The *green squares* and *gray cables* comprise the onboard readout electronics. Image credit: University of Liverpool

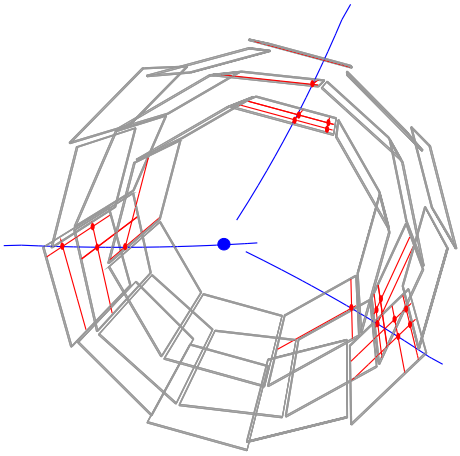

Fig. 2 Example event reconstruction in the ALPHA detector. Strips registering charge are shown as the *long red line* segments and the hit positions are given as *red ovals*. Reconstructed charged particle tracks are shown as the *blue curves* and the vertex position is shown as the *blue circle*

2 ALPHA silicon detector

The ALPHA detector (shown in Fig. 1) consists of 60 double-sided silicon detection modules arranged in three concentric tiers. Modules in the inner and middle layers are located around the trap axis at radii of 7.5 cm and 9.55 cm respectively, while modules in the outer layer are split between radii of 10.9 cm and 11.4 cm (the arrangement of detector modules can be seen in Fig. 2). The detector is split axially into two sections, each containing 30 modules. Each detector module has an active silicon area of 6 cm $\times$ 23 cm, with 256 readout strips with a pitch width of 227 μm in the azimuthal direction, and 256 readout strips with a pitch width of 875 μm in the axial direction. The signal strips run in orthogonal directions on opposite sides of the silicon wafer. This orthogonal strip geometry allows for particle 'hits' (where a particle passes through the silicon wafer) to be localized in the 3-dimensional reference frame of the detector. The total axial extent of the detector is 46 cm, which provides a solid angle coverage of $\sim$90% for annihilations in the axial center.

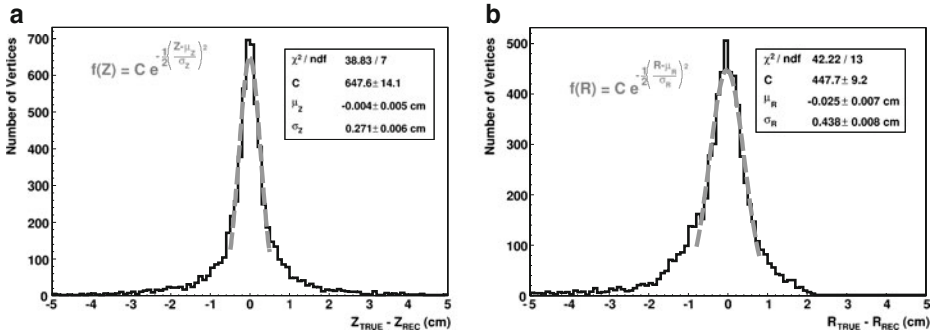

Fig. 3 Vertex position resolution, as estimated using Monte Carlo simulation. The difference between the simulated and reconstructed vertex position is shown for **a** the axial, and **b** the radial vertex coordinates. Gaussian resolution functions have been fitted to the central widths of the distributions, and are shown in *gray*

3 Event reconstruction

The ALPHA silicon tracking detector is used primarily to determine annihilation positions within the ALPHA apparatus. Positron annihilation produces two 511 keV γ-rays, which are largely attenuated and absorbed before reaching the silicon detector. Conversely, antiproton annihilation produces, on average, about three charged and two neutral pions [4]. The neutral pions quickly decay into γ-rays, which can, in turn, produce $e^- e^+$ pairs (which will often pass all the way through the detector).

The annihilation position (or 'vertex') is found by reconstructing the trajectories (or 'tracks') of charged particles that pass all the way through the detector. Figure 2 shows an example event reconstruction (an 'event' is considered to be the full triggering and readout of the detector). Here, particle tracks are found by considering combinations of three hits (shown as red boxes). The helical tracks, which model the trajectory of the charged particles in the strong axial magnetic field, are extrapolated into the trapping region near the radial center of the ALPHA apparatus. The vertex position, $\mathbf{r}_{\text{vertex}}$, is determined through the minimization of D, which is a figure of merit representing the mean distance of closest approach of the tracks to the vertex position:

$$D = \frac{1}{N_{\text{tracks}}} \sum_{i=1}^{N_{\text{tracks}}} d_i, \tag{1}$$

where N_{tracks} is the number of tracks included, and d_i is the distance of closest approach of the ith track, with track position $\mathbf{r}_i$, to the vertex position:

$$d_i^2 = \min \left\{ |\mathbf{r}_i - \mathbf{r}_{\text{vertex}}|^2 \right\}. \tag{2}$$

Tracks are extrapolated for at least 5.3 cm, and as much as ∼14 cm (the distance between the first detector layer and inner radius Penning-Malmberg trap electrodes. As particles traverse the ALPHA apparatus, they necessarily will have passed through several layers of scattering material before passing through the silicon detector. The effect of this scattering material is to increases the statistical

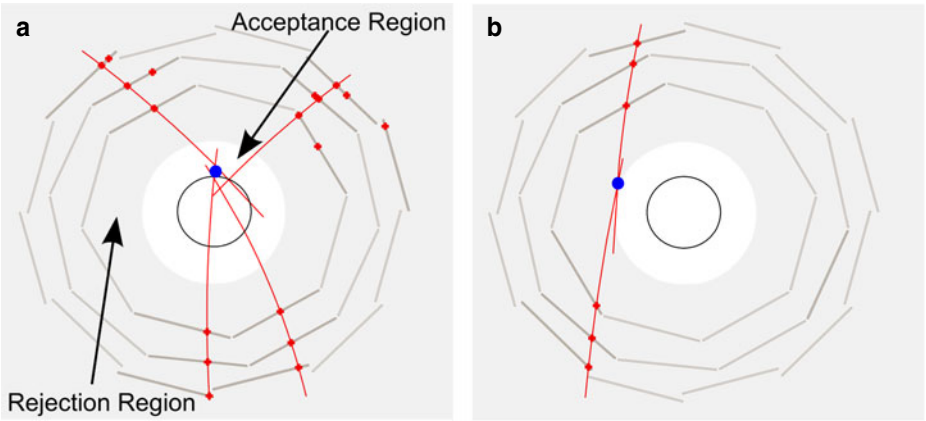

Fig. 4 A visual depiction of the vertex position radius cut, for **a** an annihilation event, and **b** a cosmic event. The *gray region* gives the region rejected by the radius cut

variance of the vertex position determination. The amount of variance, or position resolution, can be estimated using Monte Carlo simulation. Figure 3 shows the distributions of differences between the simulated and reconstruction vertex positions. The central widths of these distributions are fitted with a Gaussian resolution function. The resolution in the axial direction (the z component) is found to be $\sigma_z = (0.271 \pm 0.006)$ cm, while the resolution in the radial component of the vertex position is found to be $\sigma_R = (0.438 \pm 0.008)$ cm. The tails of the resolution distributions correspond to events where the vertex has been poorly determined.

4 Cosmic background rejection

A significant background for the vertex reconstruction comes from charged cosmic ray particles. Specifically, cosmic muons pass through and trigger the detector at a rate of about ∼10 events/s. Fortunately, most cosmic background events can be identified using several discriminating variables, including: the radial vertex position coordinate, R; and the linear residual, δ.

4.1 Vertex position radius, R

Annihilations only occur within the ALPHA apparatus—either on the inner surface of the Penning-Malmberg trap electrodes, or on background gas within the vacuum system. This physical constraint restricts the possible locations of the reconstructed vertex. That is, the radial coordinate of the annihilation vertex is expected to be inside the electrode radius (within the radial position resolution). However, a cosmic event with two co-linear tracks will return a vertex that is unconstrained in the radial coordinate. Thus, events where the vertex is found well outside of the inner apparatus radius are rejected. Figure 4 gives a visual depiction of the vertex position radius cut. An annihilation event within the cut radius is shown in Fig. 4a, and is contrasted with a cosmic event, which fails the radius cut, in Fig. 4b.

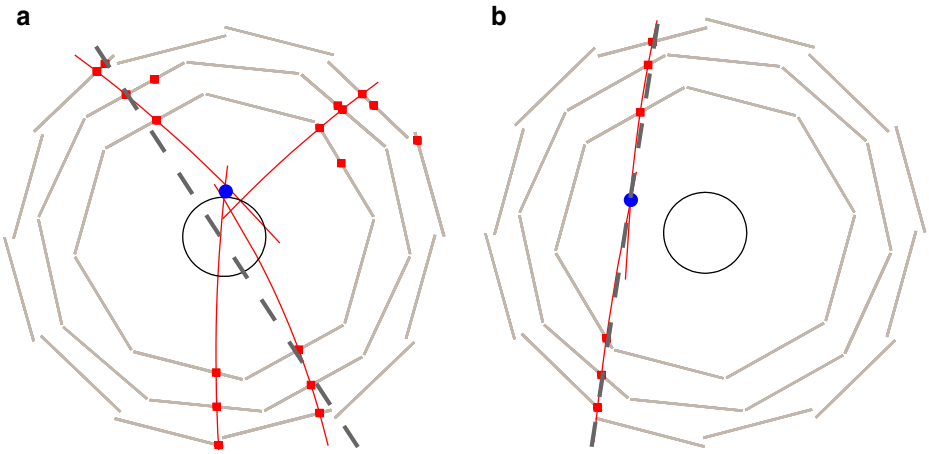

Fig. 5 A visual depiction of the linear residual cut, for **a** an annihilation event, and **b** a cosmic event. The *dashed gray line* shows the best linear fit to the hits in the event

4.2 Linear residual, δ

To first order, cosmic ray particles follow straight-line trajectories through the ALPHA detector (their curvature in the magnetic field is usually small). As such, events consistent with a single, linear, particle track are likely to have come from a cosmic particle. The combined linear residual, δ, can be used to evaluate how closely an event conforms to a single straight line track. This estimator is given as follows:

$$\delta = \min \left\{ \sum_{i \in \mathcal{F}} d_{\perp,i}^2 \right\}, \tag{3}$$

where $d_{\perp,i}$ is the perpendicular distance, or residual, between the fitted line and the i-th hit in the set of hits, $\mathcal{F}$. The minimization involves cycling through the available combinations of tracks, and is done to find the combination that gives the best linear fit. Figure 5 shows how the linear residual can differentiate between annihilation and cosmic events. Figure 5a depicts the difficulty in fitting a straight line to an annihilation event; conversely, Fig. 5b shows a cosmic event with a well-fit straight line. In this way, an event with a large δ value is likely an annihilation event.

It is important to note that cosmic ray particles do not, in general, follow straight-line trajectories (due to scattering in the apparatus material and bending in the strong magnetic fields). However, for the majority of cosmic events, departures from linearity are within the tolerance of the δ-cut (as will be shown in Section 4.3).

4.3 Signal optimization

For efficient cosmic background rejection, the cuts described in Sections 4.1 and 4.2 need to be optimized to discard cosmic events, while retaining as many annihilation

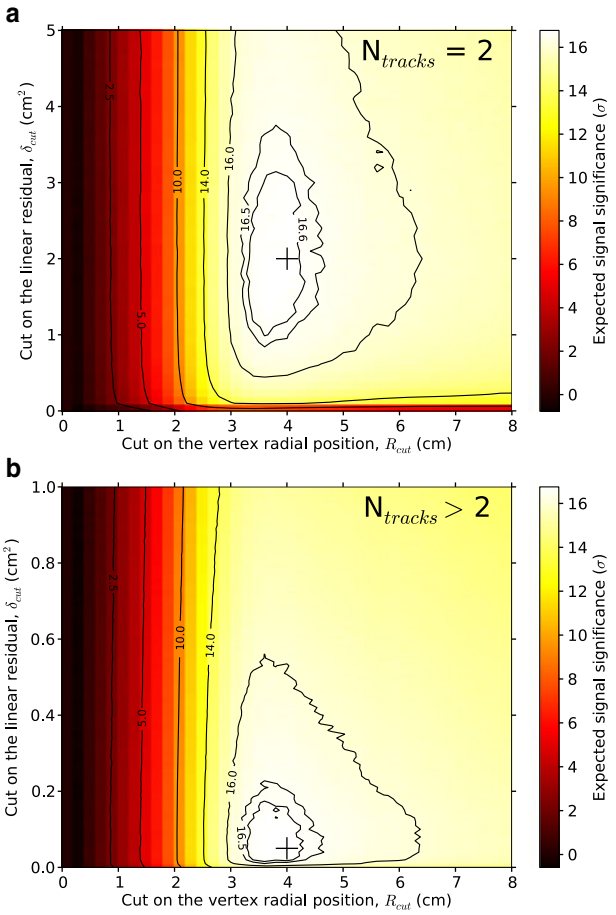

Fig. 6 The expected signal significance as a function of the cuts on the vertex radius, R_{cut}, and combined linear residual, δ_{cut}, for **a** events with $N_{\text{tracks}} = 2$, and **b** events with $N_{\text{tracks}} > 2$. The final cut decisions are shown as the *black crosses*

events as possible. Equivalently, this amounts to maximizing the signal significance, which is given by the Poisson p-value, α,

$$\alpha(n_0, b) = \sum_{n=n_0}^{\infty} \frac{b^n e^{-b}}{n!}, \tag{4}$$

where n_0 is the number of observed events with Poisson background, b. The p-value represents the probability that the observed events (or more) are entirely due to the Poisson background. Both the number of observed events and background rate are functions of the radius cut, R_{cut}, and the residual cut, δ_{cut}.

In order to avoid unintentional bias, all analyses were performed and finalized on auxiliary datasets. The signal dataset consisted of annihilation events from unconfined antihydrogen produced during the mixing of positrons and antiprotons. Conversely, the background dataset was collected by operating the detector with no antiparticles within the apparatus. The auxiliary datasets can be used to estimate the expected signal significance, α, and optimize the placement of the radius and

Table 1 Final parameter cuts. Events satisfying these cuts are classified as annihilations

N_{tracks}	Vertex radius, R_{cut} (cm)	Linear residual, δ_{cut} (cm^2)
=2	<4	>2
>2	<4	>0.05

residual cuts. The background rate (as a function of the cuts, $b = b(R_{\text{cut}}, \delta_{\text{cut}})$ can be determined by directly applying the cuts to the cosmic background dataset.

Although the expected number of observed events is also a function of the applied cuts, $n_0 = n_0(R_{\text{cut}}, \delta_{\text{cut}})$, it is difficult to estimate the expected signal rate since the antihydrogen distribution is not well characterized throughout the trapping experiments. Instead, a baseline number of expected events is taken from [5]. The expected number of events is then determined by scaling the baseline number according to the auxiliary annihilation distribution.

In order to optimize the expected signal significance, (4) is estimated over a wide range of radius and residual cuts. However, for a low-rate process such as antihydrogen trapping, n_0 is assumed to follow Poisson statistics. To reflect these statistics, an aggregate value for α is calculated (for each set of cuts) using 5000 pseudoexperiments. For each pseudoexperiment, the number of observed events is sampled from a Poisson distribution with mean $n_0(R_{\text{cut}}, \delta_{\text{cut}})$. Figure 6 shows the expected signal significance for events with two charged tracks ($N_{\text{tracks}} = 2$, Fig. 6a, and events with more than two charged tracks ($N_{\text{tracks}} > 2$, Fig. 6b. Each bin $(R_{\text{cut},i}, \delta_{\text{cut},j})$ in this figure represents an separate set of cuts, and 5,000 corresponding pseudoexperiments. The black crosses in Fig. 6 represent the final choice of cuts, which are enumerated in Table 1.

Using these cuts, $(99.54 \pm 0.02)\%$ of backgrounds events are rejected, corresponding to a background acceptance rate of $(47 \pm 2) \times 10^{-3}$ events/s. Likewise, $(64.4 \pm 0.1)\%$ of the events in the signal sample pass the cuts. Since the events included in these datasets were collected from *in situ* measurements, the resulting background rejection and signal acceptance correspond to total efficiencies, which include both the silicon and reconstruction efficiencies.

5 Conclusion

This paper describes the methods related to the reconstruction of annihilation events in the ALPHA detector. In addition, the analysis to optimize the background suppression is presented. After optimization, these algorithms permit a background rate of $(47 \pm 2) \times 10^{-3}$ events/s in the ALPHA detector, while accepting $(64.4 \pm 0.1)\%$ of annihilation events. This detector and these methods were crucial to the successful observation of trapped antihydrogen and will likely be important for future spectroscopic measurements of antihydrogen in the ALPHA apparatus. Additional details about the reconstruction and analysis will be provided in a forthcoming publication [6].

Acknowledgements This work was supported by CNPq, FINEP/RENAFAE (Brazil); ISF (Israel); MEXT (Japan); FNU (Denmark); VR (Sweden); NSERC, NRC/TRIUMF, AIF, FQRNT, and the Killam Trust (Canada); the DOE and the NSF (USA); and EPSRC, the Royal Society and the

Leverhulme Trust (UK). We would like to thank D. Seddon, J. Thornhill, and D. Wells (University of Liverpool) for their work on the construction of the vertex detector.

References

1. Andresen, G.B., et al.: Nature **468**, 673 (2010)
2. Niering, M., et al.: Phys. Rev. Lett. **84**, 5496 (2000)
3. Lüders, G.: Ann. Phys. **2**, 1 (1957)
4. Bendiscioli, G., Kharzeev, D.: Rivista Nuovo. Cim. **17**, 1 (1994)
5. Andresen, G.B., et al.: Phys. Lett. B **695**, 95 (2011)
6. Andresen, G.B., et al.: Antihydrogen annihilation reconstruction with the ALPHA silicon detector. Nucl. Instr. Methods Phys. Res. A (2011, submitted)